JOURNAL OF THERMOPHYSICS AND HEAT TRANSFER
Vol. 12, No. 1, January–March 1998

Condensation in Rotating Stepped Wall Heat Pipes with Hysteretic Annular Flow

Lanchao Lin* and Amir Faghri†
University of Connecticut, Storrs, Connecticut 06269-3139

Hysteresis effects of annular flow in rotating stepped wall heat pipes are addressed based on visualization and systematic experiments. The region of hysteretic annular flow is defined. Experimental data relating the condensation heat transfer for annular flow in a rotating stepped wall heat pipe are presented. A model for predicting the condensation heat transfer coefficient is proposed. The theoretical result is compared with experimental data. The effect of vapor shear drag on the condensation heat transfer is discussed.

Nomenclature

A_c = inner wall area of condenser cylinder, m^2
A_v = cross-sectional area of vapor flow passage, m^2
Ca = capillary number, $\mu_l^2 gR/\sigma^2$
D_r = liquid loading, $\bar{\delta}/R$
E = specific energy, J kg^{-1}
Fr = Froude number, $\omega^2 R/g$
f = friction coefficient
Ga = Galileo number, $\rho_l^2 gR^3/\mu_l^2$
g = gravitational acceleration, m s^{-2}
h_c = condensation heat transfer coefficient, W m^{-2} K^{-1}
h_{fg} = latent heat of evaporation, J kg^{-1}
k = thermal conductivity, W m^{-1} K^{-1}
L = length, m
$\dot{m}$ = mass flow rate, kg s^{-1}
N = rotational speed, rpm
p = pressure, N m^{-2}
Q = heat rate (output), W
Q_{in} = input heat rate, W
R = inner radius of condenser, m
Re_v = vapor Reynolds number, $2R\rho_u \bar{w}_v/\mu_v$
T_v = vapor temperature, °C
T_{wi} = inner wall temperature, °C
T_{wo} = outer wall temperature, °C
V^+ = fill ratio
w = axial velocity, ms^{-1}
y = radial coordinate, m
z = axial coordinate, m
Γ_l = liquid mass flow rate per unit width, kg m^{-1} s^{-1}
δ = liquid film thickness, m
δ_w = wall thickness, m
μ = dynamic viscosity, N s m^{-2}
ρ = mass density, kg m^{-3}
σ = surface tension, N m^{-1}
$\tau_{v,\delta}$ = interfacial shear stress, N m^{-2}
ω = angular velocity, rad s^{-1}

Subscripts
a = adiabatic section
c = condenser
l = liquid
s = position at the step
v = vapor
w = wall
δ = liquid–vapor interface

Superscript
$-$ = mean value

Received Oct. 18, 1996; revision received May 9, 1997; accepted for publication May 15, 1997.

*Research Associate, Department of Mechanical Engineering; currently at Department of Mechanical and Materials Engineering, Wright State University, Dayton, OH 45435.
†Professor and Head, Department of Mechanical Engineering.

Introduction

IN rotating heat pipes, the thermal energy transport relies on the evaporation and condensation of a small amount of working fluid, whereas the condensate return relies on centrifugal force. The general concept of the rotating heat pipe was first formulated by Gray.[1] Since that time, many investigations have been made on fluid heat transfer characteristics in both the evaporator and condenser sections.[2]

Ballback[3] extended the Nusselt-type analysis for film condensation on the inside of a rotating truncated cone by assuming that the liquid film was very thin and had a slope much smaller than the cone angle. By neglecting the vapor shear stress, he obtained a closed-form expression for the total heat transfer from the condenser. The problem associated with the interfacial shear stress was addressed by Daniels and Al-Jumaily.[4] A variable shear-stress formulation was incorporated into the condensate film flow analysis for a rotating heat pipe. Daniels and Al-Jumaily carried out an experimental investigation, where the results showed good agreement for the Arcton 113 and 21 fluids, but no agreement with water. Marto[5] performed an analysis similar to that of Daniels and Al-Jumaily[4] for the condensation heat transfer in a rotating heat pipe. The analysis by Marto[5] included the effect of the vapor pressure drop in the condenser. Marto concluded that the performance of rotating heat pipes could be improved by using thin-walled condensers made of high conductivity materials. Salinas and Marto[6] solved a conjugate heat transfer problem involving conduction heat transfer in the wall and film condensation on the inside of a finned rotating heat pipe, using a finite element technique. It was concluded that two-dimensional effects influenced the local heat flux distribution within the fins and the wall. With the proposed method, an optimum fin configuration could be determined for a given set of operating conditions. Faghri et al.[7] performed a more complete rotating heat pipe vapor flow analysis using a two-dimensional model. They found a reverse flow region at the centerline for high rotational speeds and, therefore, conventional pressure drops and shear-stress correlations do not apply in rotating heat pipes for high rotational speeds. More recently, a complete transient two-dimensional model of a rotating heat pipe was presented by Harley and Faghri.[8] The thin liquid film was coupled to the two-dimensional vapor velocity at the liquid–vapor

interface, and the effects of the vapor pressure drop and the interfacial shear stress were included.

In addition to the previously mentioned investigations on annular flow, attention was paid to other flow patterns. Katsuta et al.[9] classified the flow inside a rotating heat pipe into four distinct patterns that are primarily dependent on Fr. Several wall configurations of rotating heat pipes have been developed, such as tapped wall, cylindrical wall, stepped wall, or a combination of wall types. Because of its favorable thermal performance at high rotational speeds and its relatively simple configuration, the stepped wall rotating heat pipe is considered an efficient heat transfer element for rotating machines. Numerous investigations on the heat transfer in stepped wall rotating heat pipes were made.[10–12] More investigations were made on the annular flow at higher rotational speeds.[4,5,10] The hysteresis phenomenon of annular flow at relatively low rotational speeds was reported,[9,11,12] but not systematically investigated. The region of hysteretic annular flow was defined as a rotational speed range between the two distinct rotational speeds corresponding to the onset and collapse of annular flow. No comparison between the theoretical results and experimental data was made in this region. Since the hysteresis state of annular flow is evident over a certain range of rotational speeds, it is necessary to study this state systematically.

The purpose of this paper is to characterize the hysteresis state of annular flow and to compare the experimental data of condensation heat transfer with a comprehensive theoretical model.

Experimental Results

Visual Observation

The hysteresis phenomenon of annular flow was found during visualization experiments,[12] reflected by two distinct rotational speeds corresponding to the onset and collapse of annular flow. The visualization experiment for the determination of basic flow patterns was carried out using a glass cylindrical wall heat pipe with a length of 540 mm, an i.d. of 42 mm, and a wall thickness of 2.5 mm. A plated layer of transparent tin oxide for electric heating was on the external surface of the evaporator. Lengths of the evaporator and condenser were 270 and 220 mm, respectively. The electric power was supplied through a pair of slip rings. The heat was removed from the condenser by a water spray. The glass heat pipe was rotated by a variable speed motor. The operating temperature was monitored by a thermocouple inserted into a small glass tube centered at the end of the condenser. Water was used as the working fluid, with a fill ratio (liquid volume divided by heat pipe internal volume) ranging from 5 to 15%.

Basic flow patterns in the glass cylindrical wall heat pipe were the stratified flow at low rotational speeds and annular flow at higher rotational speeds (Fig. 1). A cellular flow could occur as the rotational speed was increased from the stratified flow to annular flow. However, the region of cellular flow was narrow and it was neglected. In the case of stratified flow, most of the liquid lay at the bottom of the rotating heat pipe, and only a small amount flowed around the inner wall, forming a thin film. Annular flow was characterized by an annular liquid body and it was mainly controlled by centrifugal force. The speed region corresponding to the hysteretic annular flow can

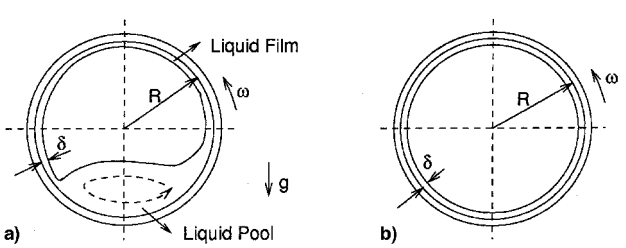

Fig. 1 a) Stratified and b) annular flows in a rotating cylindrical wall heat pipe.

be determined by critical conditions for the onset and collapse of annular flow. The onset rotational speed of annular flow is a transitional speed from the stratified to annular flow. The rotational collapse speed of the annular flow is that of the transition from the annular to stratified flow. The empirical correlation for predicting the onset rotational speed for annular flow proposed by Ohtsuka et al.[13] can be written as

$$Fr = 15.96 Ga^{0.107} Ca^{-0.08} (L/2R)^{-0.21} (V^+)^{0.91} \tag{1}$$

To determine the rotational speed at which the annular flow collapses, a simple relation derived by Lin and Groll[14] can be used:

$$Fr = \frac{3}{(1 - D_r)^2} \tag{2}$$

The rotational speed corresponding to the collapse of the annular flow could be much lower than that corresponding to the onset of annular flow in the case of large fill ratio; e.g., larger than 9%. The hysteresis is believed to be a result of a secondary flow in the liquid pool (Fig. 1). The secondary flow circulates in the same direction as ω, and prevents the liquid pool from being dragged up onto the turning wall.

In the state of hysteretic annular flow at relatively low rotational speeds, there existed a circumferential variation of the liquid film thickness caused by the effect of gravitational force. Near the critical condition for collapse of the annular flow, the hysteretic annular flow was characterized by a noticeable three-dimensional flow pattern with an axially wavy liquid–vapor interface.[14] Note that the hysteretic annular flow remained stable, even if the rotational speed of the glass heat pipe with 9% fill ratio was dramatically decreased from 1400 to 500 rpm within a time interval of 2.5 s, and then maintained at 500 rpm after 2.5 s.

The visualization experiment using a glass stepped wall heat pipe was also conducted under the same experimental conditions for comparison with the case of the glass cylindrical wall heat pipe. Lengths of the evaporator and condenser were 225 and 280 mm, respectively. Inner diameters of the evaporator and condenser were 42 and 36 mm, respectively. The wall thickness was 2.5 mm. It was shown that the basic flow patterns and the hysteresis phenomenon in the glass stepped wall heat pipe were the same as those in the glass cylindrical wall heat pipe. Distinct phenomena of the glass stepped wall heat pipe with the fill ratio smaller than 15% are discussed next. As the rotational speed approached the onset rotational speed for the annular flow in the condenser, more and more liquid in the condenser moved in the evaporator until there was only a thin condensate film around the condenser wall. If the annular flow was transferred into the stratified flow by decreasing the rotational speed, the annular flow in the evaporator collapsed, and this caused the immediately collapse of the annular liquid film in the condenser.

Performance Test

The dimensions and structure of the stepped wall heat pipe plus temperature measuring positions are shown in Fig. 2. This prototype heat pipe was used in the system experiment.[12] Water was used as the working fluid. The heat pipe wall material was carbon–steel. The inner wall surface was pretreated and a thin layer of Fe_3O_4 was formed on the inner surface. Figure 3 demonstrates the schematic of the test apparatus. In the evaporator, a nichrome wire heater was uniformly wound on the heat pipe. In the condenser, a tube with circular aluminum fins (fin thickness 1.2 mm and fin density 2.5/cm) was installed, and the heat pipe was cooled by forced air crossflow. The flow rate could be adjusted by a valve and measured through a pressure manometer. For temperature measurement, five thermocouples were placed on the wall surface along the evaporator and six

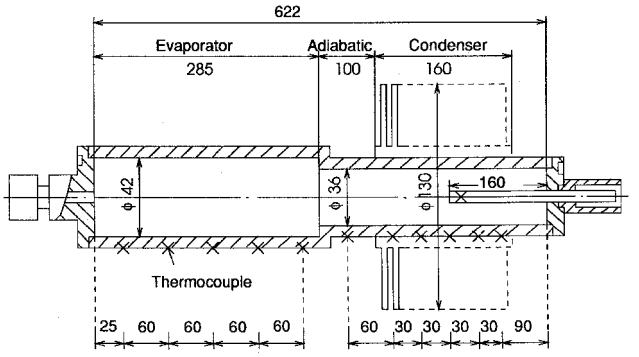

Fig. 2 Longitudinal section of the rotating stepped wall heat pipe[12] (dimensions in millimeters).

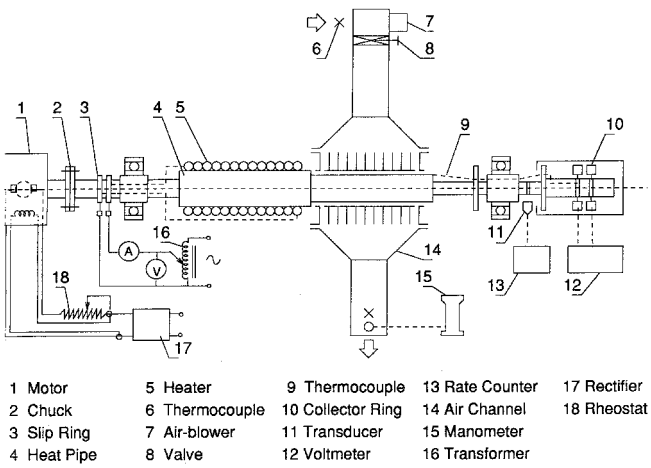

Fig. 3 Schematic of test apparatus.[12]

thermocouples along the condenser. One thermocouple was installed in the small center tube to measure the vapor temperature. All thermocouples were led to a ring collector composed of 12 silver rings connected to a digital voltmeter. Thermocouples were calibrated at rotational speeds from 0 to 1600 rpm. In most cases, the heat losses in the experiment, defined as $(Q_{in} - Q)/Q_{in}$, were controlled within 25%.

The difference of the vapor temperature measured along the center tube was less than 0.05°C, which was neglected. The measured temperature at the end of the center tube was defined as the operating temperature T_v. The experimental condensation heat transfer coefficient was estimated by

$$h_c = \frac{Q}{2\pi R L_c (T_v - \bar{T}_{wi,c})} \tag{3}$$

where the average condenser inner wall temperature $\bar{T}_{wi,c}$ was calculated by

$$\bar{T}_{wi,c} = \bar{T}_{wo,c} - \frac{Q\delta_{w,c}}{2\pi(R + 0.5\delta_{w,c})L_c k_w} \tag{4}$$

where $\bar{T}_{wo,c}$ was the arithmetic average of the temperatures measured at the outer wall of the condenser. The overall uncertainty for h_c was investigated, and it was found that the uncertainty of h_c was 11.0%, which occurred at a low heat rate of 200 W and a rotational speed of 1200 rpm.

The experimental data, with error bars, regarding the condensation heat transfer coefficient of the annular flow vs rotational speed at the operating temperature of 70°C, are presented in Fig. 4 (see Ref. 13). Points with the symbol, ○, refer to the hysteretic annular flow since the stratified flow is available in the rotational speed range corresponding to these points with ○. With the exception of the data at 500 rpm, the condensation heat transfer coefficient for annular flow increases with any rotational speed increase. At the same rotational speed, a higher heat rate results in a lower heat transfer coefficient because of a rise in condensate mass flow rate. Notice that the condensation heat transfer coefficient for the stratified flow is much higher than that for the hysteretic annular flow. The high h_c for the stratified flow is attributed to the thin liquid film behavior on the upper part of the wall.

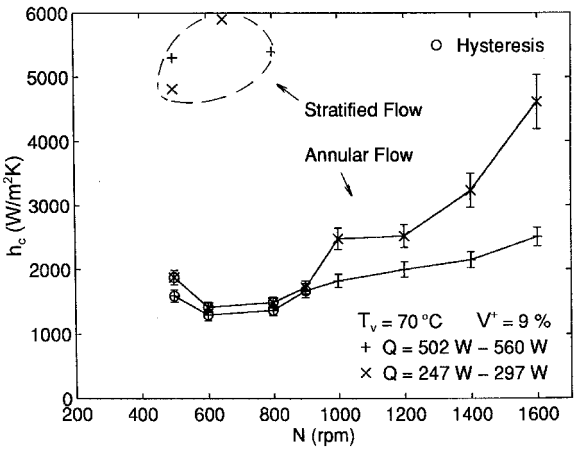

Fig. 4 Effect of the rotational speed on condensation heat transfer coefficient of the annular flow in the rotating stepped wall heat pipe.

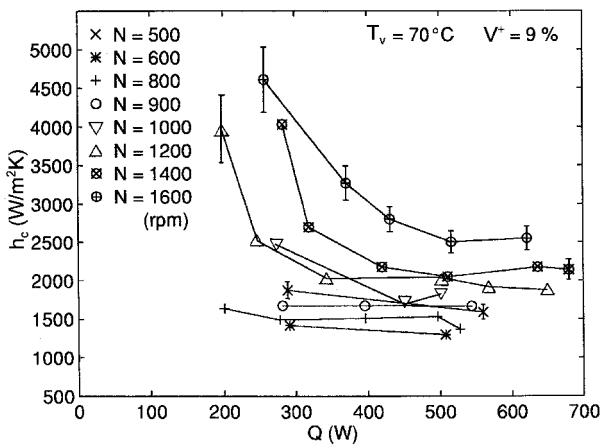

Fig. 5 Condensation heat transfer coefficient as a function of heat rate and rotational speed (error bars presented for the upper and lower bounds of the rotational speed and heat rate).

Figure 5 shows the condensation heat transfer coefficient as a function of heat rate and rotational speed. In most cases, the heat transfer coefficient decreases with any heat rate increase, and this coefficient increases with a rotational speed increase at the same heat rate, except for the data at N = 500 rpm, which is near the collapse condition of annular flow.

Analysis and Comparison with Experimental Data

In the cylindrical section including condenser and adiabatic zones with a step at the position connecting the evaporator, the condensate return is maintained by centrifugal forces acting on the liquid film with varying film thickness, which results in a hydrostatic pressure change in the film. The coordinate system for annular flow is shown in Fig. 6.

The assumptions made in the present analysis of condensate film are as follows:

1) The condensate film flow is laminar.

2) Liquid subcooling is negligible.

3) The liquid film thickness is much smaller than the heat pipe inner radius.

4) The radial heat flux is uniform.

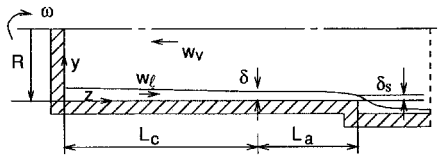

Fig. 6 Coordinates for annular flow in condenser and adiabatic sections of a rotating stepped wall heat pipe.

5) Inertial and convective effects in the liquid are neglected.
6) The gravitational force is negligible compared to the centrifugal force.

The momentum equations in the y and z directions for liquid flow are

$$\frac{\partial p}{\partial y} = -\rho_l \omega^2 (R - y) \tag{5}$$

$$\frac{\partial p}{\partial z} = \mu_l \frac{\partial^2 w_l}{\partial y^2} \tag{6}$$

with the following boundary conditions:

$$y = 0, \qquad w_l = 0 \tag{7}$$

$$y = \delta, \qquad \mu_l \left(\frac{\partial w_l}{\partial y}\right)_{y=\delta} = -\tau_{v,\delta} - \frac{d\Gamma_l}{dz}(\bar{w}_v + w_{l,\delta}) \tag{8}$$

$$y = \delta, \qquad p = p_v \tag{9}$$

The interfacial shear stress $\tau_{v,\delta}$ in Eq. (8) is calculated by

$$\tau_{v,\delta} = (f/2)\rho_v \bar{w}_v^2 \tag{10}$$

where f is calculated according to the conventional pipe flow correlations:

$$f = \frac{16}{Re_v} \qquad Re_v \le 2000 \tag{11}$$

$$f = \frac{0.079}{Re_v^{0.25}} \qquad Re_v > 2000 \tag{12}$$

with

$$Re_v = \frac{2R\rho_v \bar{w}_v}{\mu_v} \tag{13}$$

and the average vapor velocity is

$$\bar{w}_v = \frac{\dot{m}_l}{\rho_v A_v} \tag{14}$$

with $A_v \approx \pi R^2$. Assuming that the mean vapor velocity $\bar{w}_v$ is much higher than the liquid–vapor interface, results in

$$\bar{w}_v + w_{l,\delta} \approx \bar{w}_v \tag{15}$$

Integrating Eq. (5) and using Eq. (9), yields

$$p_l = p_v + \rho_l \omega^2 [R(\delta - y) - \tfrac{1}{2}(\delta^2 - y^2)] \tag{16}$$

Differentiating Eq. (16) with respect to z, yields

$$\frac{\partial p_l}{\partial z} = \rho_l \omega^2 (R - \delta)\frac{d\delta}{dz} + \frac{dp_v}{dz} \tag{17}$$

Substituting the preceding pressure relation into the z-direction momentum, Eq. (6) results in

$$\mu_l \frac{\partial^2 w_l}{\partial y^2} = \rho_l \omega^2 (R - \delta)\frac{d\delta}{dz} + \frac{dp_v}{dz} \tag{18}$$

Solving Eq. (18) with the boundary conditions, Eqs. (7) and (8), yield

$$w_l = -\frac{\rho_l \omega^2}{\mu_l}(R - \delta)\left(\delta y - \frac{y^2}{2}\right)\frac{d\delta}{dz} - \frac{y}{\mu_l}\left(\tau_{v,\delta} + \frac{d\Gamma_l}{dz}\bar{w}_v\right) - \frac{1}{\mu_l}\frac{dp_v}{dz}\left(\delta y - \frac{y^2}{2}\right) \tag{19}$$

The mass flow rate of the liquid condensate is

$$\dot{m}_l = \int_0^\delta 2\pi (R - y)\rho_l w_l \, dy \tag{20}$$

Substituting Eq. (19) into Eq. (20), the following is obtained:

$$\dot{m}_l = -\frac{2\pi\rho_l^2 \omega^2 R(R - \delta)}{\mu_l}\left(\frac{\delta^3}{3} - \frac{5}{24}\frac{\delta^4}{R}\right)\frac{d\delta}{dz} - \frac{2\pi\rho_l R}{\mu_l}\left(\tau_{v,\delta} + \frac{d\Gamma_l}{dz}\bar{w}_v\right)\left(\frac{\delta^2}{2} - \frac{\delta^3}{3R}\right) - \frac{dp_v}{dz}\frac{2\pi\rho_l R}{\mu_l}\left(\frac{\delta^3}{3} - \frac{5}{24}\frac{\delta^4}{R}\right) \tag{21}$$

Under the assumption that $\delta << R$, Eq. (21) can be written as follows:

$$\frac{d\delta}{dz} = -\frac{3\mu_l}{2\pi\rho_l^2 \omega^2 R^2 \delta^3}\left[\dot{m}_l + \frac{\pi\rho_l R}{\mu_l}\left(\tau_{v,\delta} + \frac{d\Gamma_l}{dz}\bar{w}_v\right)\delta^2 + \frac{dp_v}{dz}\frac{2\pi\rho_l R\delta^3}{3\mu_l}\right] \tag{22}$$

Under the assumption of a uniform condensation heat flux and negligible liquid subcooling, the mass flow rates in the adiabatic and condenser sections can be expressed as:

$$\dot{m}_l = \frac{Q}{h_{fg}} \qquad L_c < z \le L_c + L_a \tag{23}$$

$$\dot{m}_l = \frac{Q}{h_{fg}}\frac{z}{L_c} \qquad 0 \le z \le L_c \tag{24}$$

The rate of condensation ($d\Gamma_l/dz$) can be related to the change in the axial mass flow rate of liquid:

$$\frac{d\Gamma_l}{dz} = \frac{L_c}{A_c}\frac{d\dot{m}_l}{dz} \tag{25}$$

where $A_c = 2\pi R L_c$.

The vapor pressure drop for $\delta << R$ can be expressed as follows (Ref. 2):

$$\frac{dp_v}{dz} = 2\frac{\tau_{v,\delta}}{R} - 2\rho_v \bar{w}_v \frac{d\bar{w}_v}{dz} \tag{26}$$

The boundary condition with respect to Eq. (22) is

$$z = L_c + L_a, \qquad \delta = \delta_s \tag{27}$$

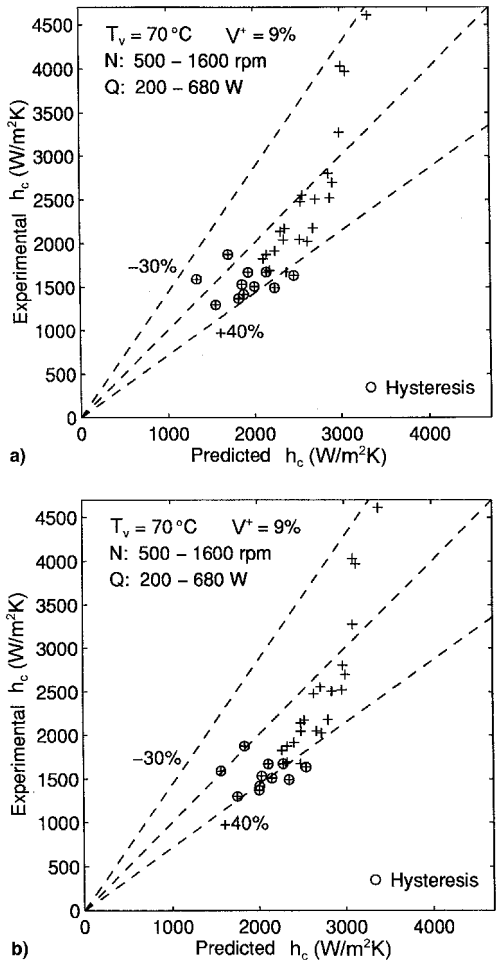

Fig. 7 Comparison of the predicted condensation heat transfer coefficient with experimental data a) with and b) without the vapor drag effect.

where δ_s is the film thicknesses at the step. At the step ($z = L_c + L_a$), the specific energy of liquid flow reaches its minimum value. This condition can be used for determining δ_s. The specific energy of liquid flow is

$$E = \omega^2 R\delta_s + (\bar{w}_{l,s}^2/2) \tag{28}$$

where

$$\bar{w}_{l,s} = \frac{Q}{2\pi R\delta_s \rho_l h_{fg}} \tag{29}$$

Minimizing E gives the film thickness at the step, similar to the free overfall of open channel flow[10,15]:

$$\delta_s = \left(\frac{Q}{2\pi\omega\rho_l h_{fg}}\right)^{2/3} \frac{1}{R} \tag{30}$$

Solving Eq. (22) subject to Eq. (27) will give the film thickness as a function of the axial position in the condenser. The average film thickness in the condenser is calculated by

$$\bar{\delta}_c = \frac{1}{L_c}\int_0^{L_c} \delta \, dz \tag{31}$$

The condensation heat transfer coefficient is defined as

$$h_c = k_l/\bar{\delta}_c \tag{32}$$

Notice that h_c does not include the influence of the fill ratio. Therefore, the present model is valid for the case where there is no excess liquid remaining in the condenser during operation. This condition corresponds to $V^+ < 13.8\%$. Under given operating conditions such as vapor temperature, heat rate, and rotational speed, the average film thickness and heat transfer coefficient in the condenser are estimated based on Eqs. (22), (27), (31), and (32). The Runge–Kutta procedure is used to solve Eq. (22). The predicted average film thickness in the condenser $\bar{\delta}_c$ ranges from 0.20 to 0.49 mm under the operating conditions similar to those of the systematic experiment (Figs. 4 and 5). The predicted condensation heat transfer coefficients are compared with the corresponding experimental results at the vapor temperature of 70 deg (Fig. 7a). The predicted heat transfer coefficients lie within −30 and +40% of the experimental data. The data with the symbol ○ refer to the hysteretic annular flow. The predicted theoretical results in the region of hysteretic annular flow are somewhat higher than the corresponding experimental ones. The reason for this could be that in the hysteretic annular flow, the counterflowing vapor exerts a higher shear stress on the wavy liquid film surface than that on a smooth surface, and this effect is not included in the modeling. With the exception of the three data for $N \geq 1200$ rpm and $Q \leq 283$ W, Fig. 7a shows that the present model of the condensation heat transfer for annular flow overpredicts the condensation heat transfer coefficient by 12% in the sense of overall average.

To understand the influence of the vapor drag on the heat transfer coefficient, these coefficients, without including the vapor drag effect, are calculated by using a boundary condition at the liquid–vapor interface $(\partial w_l/\partial y)_{y=\delta} = 0$, instead of using Eq. (8), and by setting $\tau_{v,\delta} = 0$. Comparison of the calculated results with the experimental data is shown in Fig. 7b. It can be seen from Fig. 7 that at relatively high heat rates (corresponding to low condensation heat transfer coefficients), the calculated condensation heat transfer coefficients without including the vapor drag effect are approximately 10% higher than those from the present model, resulting in greater discrepancy from the experimental results. The vapor drag decreases the condensation heat transfer coefficient since the liquid film tends to thicken under the influence of the counterflowing vapor. This effect is more noticeable at lower rotational speeds since the liquid film is thicker and, thus, has a smaller opposing resistance to the vapor shear.

Conclusions

The following conclusions may be drawn from the experiments and analysis.

1) The hysteretic annular flow is a stable flow pattern. The hysteresis principally results from a secondary flow in the liquid pool.

2) The condensation heat transfer coefficient in the hysteretic annular flow region are relatively low compared to the data in the other region. This is partially because the counterflowing vapor causes a greater shear stress at the wavy liquid film surface in the hysteretic annular flow region and, consequently, results in a thicker liquid film with a lower heat transfer coefficient.

3) The calculated condensation heat transfer coefficients at relatively high rotational speeds are approximately 10% lower from the present model than from the model without accounting for the vapor drag.

4) In most cases, the present model of the condensation heat transfer for annular flow overpredicts the condensation heat transfer coefficient by 12%. The discrepancy from the experimental data is within −30 and +40%.

Acknowledgments

The experimental work was carried out at the Nanjing Institute of Chemical Technology, People's Republic of China,

and it was financed by the National Economic Committee of China.

References

[1]Gray, V. H., "The Rotational Heat Pipe—A Wickless Hollow Shaft for Transferring High Heat Fluxes," American Society of Mechanical Engineers, Paper 69-HT-19, 1969.

[2]Faghri, A., *Heat Pipe Science and Technology*, Taylor and Francis, Washington, DC 1995.

[3]Ballback, L. J., "The Operation of a Rotating Wickless Heat Pipe," M.S. Thesis, U.S. Naval Postgraduate School, AD 701674, Monterey, CA, 1969.

[4]Daniels, T. C., and Al-Jumaily, F. K., "Investigations of the Factors Affecting the Performance of a Rotating Heat Pipe," *International Journal of Heat and Mass Transfer*, Vol. 18, 1975, pp. 961–973.

[5]Marto, P. J., "Performance Characteristics of Rotating Wickless Heat Pipes," *Proceedings of the 2nd International Heat Pipe Conference* (Bologna), 1976.

[6]Salinas, D., and Marto, P. J., "Analysis of an Internally Finned Rotating Heat Pipe," *Numerical Heat Transfer*, Vol. 19, No. 3, 1991, pp. 255–275.

[7]Faghri, A., Gogineni, S., and Thomas, S., "Vapor Flow Analysis of an Axially Rotating Heat Pipe," *International Journal of Heat and Mass Transfer*, Vol. 36, No. 9, 1993, pp. 2293–2303.

[8]Harley, C., and Faghri, A., "Two-Dimensional Rotating Heat Pipe Analysis," *Journal of Heat Transfer*, Vol. 117, No. 1, 1995, pp. 202–208.

[9]Katsuta, M., Kigami, H., Nagata, K., Sotani, J., and Koizumi, T., "Performance and Characteristics of a Rotating Heat Pipe," *Proceedings of the 5th International Heat Pipe Conference* (Tsukuba), 1984.

[10]Vasiliev, L. L., and Khrolenok, V. V., "Heat Transfer in Rotating Heat Pipes," *Proceedings of the 7th International Heat Pipe Conference* (Minsk), 1990.

[11]Nakayama, W., Ohtsuka, Y., and Yoshikawa, T., "The Effects of Fine Surface Structures on the Performance of Horizontal Rotating Heat Pipes," *Proceedings of the 5th International Heat Pipe Conference* (Tsukuba), 1984.

[12]Lin, L., "Heat Transfer Mechanism in a Rotating Heat Pipe with Stepped Wall," M.S. Thesis, 0033, Nanjing Inst. of Chemical Technology, Nanjing, PRC, Dec., 1986.

[13]Ohtsuka, Y., Nakayama, W., and Yoshikawa, T., "Performance of Horizontal Rotating Heat Pipes (Part 1)," *Transactions of the Japan Society of Mechanical Engineers, Fluids and Thermal Engineering*, Vol. 50, 1984, pp. 2162–2170.

[14]Lin, L., and Groll, M., "Critical Conditions for Collapse of Annular Flow in a Rotating Heat Pipe with a Cylindrical Wall," *Heat Transfer Engineering*, Vol. 17, No. 3, 1996, pp. 29–34.

[15]Blevins, R. D., *Applied Fluid Dynamics Handbook*, Reinhold, New York, 1984.